Available online at www.sciencedirect.com
SCIENCE DIRECT®
Experimental Thermal and Fluid Science 30 (2006) 345–354
Experimental Thermal and Fluid Science
www.elsevier.com/locate/etfs

# Flow pattern, pressure drop and void fraction of two-phase gas–liquid flow in an inclined narrow annular channel

Somchai Wongwises *, Manop Pipathattakul

*Fluid Mechanics, Thermal Engineering and Multiphase Flow Research Lab (FUTURE), Department of Mechanical Engineering, King Mongkut's University of Technology Thonburi, Bangmod, Bangkok 10140, Thailand*

Received 1 July 2005; accepted 16 August 2005

**Abstract**

Two-phase flow pattern, pressure drop and void fraction in horizontal and inclined upward air–water two-phase flow in a mini-gap annular channel are experimentally studied. A concentric annular test section at the length of 880 mm with an outer diameter of 12.5 mm and inner diameter of 8 mm is used in the experiments. The flow phenomena, which are plug flow, slug flow, annular flow, annular/slug flow, bubbly/plug flow, bubbly/slug–plug flow, churn flow, dispersed bubbly flow and slug/bubbly flow, are observed and recorded by high-speed camera. A slug flow pattern is found only in the horizontal channel while slug/bubbly flow patterns are observed only in inclined channels. When the inclination angle is increased, the onset of transition from the plug flow region to the slug flow region (for the horizontal channel) and from the plug flow region to slug/bubbly flow region (for inclined channels) shift to a lower value of superficial air velocity. Small shifts are found for the transition line between the dispersed bubbly flow and the bubbly/plug flow, the bubbly/plug flow and the bubbly/slug–plug flow, and the bubbly/plug flow and the plug flow. The rest of the transition lines shift to a higher value of superficial air velocity. Considering the effect of flow pattern on the pressure drop in the horizontal tube at low liquid velocity, the occurrence of slug flow stops the rise of pressure drop for a short while, before rising again after the air velocity has increased. However, the pressure does not rise abruptly in the tubes with $\theta = 30°$ and 60° when the slug/bubbly flow occurs. At low gas and liquid velocity, the pressure drop increases, when the inclination angles changes from horizontal to 30° and 60°. Void fraction increases with increasing gas velocity and decreases with increasing liquid velocity. After increasing the inclination angle from horizontal to $\theta = 30°$ and 60°, the void fraction appears to be similar, with a decreasing trend when the inclination angle increases.


*Keywords:* Two-phase flow; Mini-channel; Narrow annular channel; Flow pattern; Pressure drop; Void fraction

## 1. Introduction

Two-phase gas–liquid flow through a confined gap is encountered in several engineering applications including boiling behavior in minichannels, cooling systems of various types of equipment such as high performance microelectronics, supercomputers, high-powered lasers, medical devices, high heat-flux compact heat exchangers in spacecraft and satellites etc. It can be expected that the restriction of the bubble space in the minichannel is the cause of the differences in the two-phase flow characteristics from those in conventional channel geometries. This may also affect heat-mass transfer characteristics during the change of phase.

It is not possible to understand the two-phase flow phenomena without a clear understanding of the flow patterns encountered. It is expected that the flow patterns will influence the two-phase pressure drop, holdup, system stability, exchange rates of momentum, heat and mass during the phase-change heat transfer processes. The ability to accurately predict the type of flow is necessary before relevant calculation techniques can be developed.

* Corresponding author. Tel.: +662 470 9115; fax: +662 470 9111.
*E-mail address:* somchai.won@kmutt.ac.th (S. Wongwises).

0894-1777/$ - see front matter © 2005 Elsevier Inc. All rights reserved.
doi:10.1016/j.expthermflusci.2005.08.002

Two-phase flow patterns in small circular tubes have been studied by a number of researchers while those in mini non-circular channels have received comparatively little attention in literature.

Zhao and Rezkallah [1] proposed the phasic Weber as system parameters to elucidate the effects of inertia and surface tension in micro-channels at micro-gravity. Their flow regime map was divided into three zones: surface tension-dominated zone (bubbly and slug flow regimes), inertia-dominated zone (annular flow regime), and the transition zone.

Wilmarth and Ishii [2,3] observed the flow patterns and measured the void fraction and the interfacial area concentration of adiabatic co-current vertical and horizontal air–water flow in narrow rectangular channels with gaps of 1 and 2 mm. The developed flow regime maps were compared with those obtained for a round pipe.

Bonjour and Lallemand [4] performed experiments to elucidate the flow regimes of natural convective boiling of R113 in upward two-phase flow in vertical narrow rectangular channels with gap sizes ranging between 0.5 and 2 mm. Three flow boiling regimes, namely nucleate boiling with isolated deformed bubbles, nucleate boiling with coalesced bubbles, and partial dry out, were observed. A new flow regime map based on the Bond number and a ratio of the heat flux to the critical heat flux was developed to confine the boiling.

Xu et al. [5,6] investigated an adiabatic co-current vertical two-phase flow of air and water in vertical rectangular channels ($12 \times 260$ mm) with narrow gaps of 0.3, 0.6 and 1.0 mm. Flow patterns for gaps of 0.6 and 1.0 mm were similar to those reported in the literature. By decreasing the channel gaps, the transition from one flow regime to another appeared at a lower gas velocity. However, for the gaps of 0.3 mm, even at very low gas flow rates, bubbly flow was never found.

Hibiki and Mishima [7] developed a mathematical model to predict the flow regime transition for vertical upward flows in narrow rectangular channels. The model was based on that of Mishima and Ishii [8] for vertical upward two-phase flows in round tubes. The developed model was compared with the measured data of air–water flows in rectangular channels with gaps of 0.3–17 mm.

Zhao and Bi [9] conducted experiments to visualize the co-current upward air–water two-phase flow patterns in vertical equilateral triangular channels with hydraulic diameters of 0.866 mm, 1.443 mm and 2.886 mm. The observed flow patterns obtained from the larger hydraulic diameters (1.443 mm and 2.886 mm) were found to be similar to those obtained from conventional, large-sized vertical circular tubes. For the smallest channel (0.866 mm), the dispersed bubbly flow pattern was not found.

Akbar et al. [10] compared the measured data reported in open literature with a Weber number-based two-phase flow regime map which was previously developed by Zhao and Rezkallah [1], and Rezkallah [11]. Balasubramanian and Kandlikar [12] used high speed photography for the observation of flow behaviors (nucleate boiling, slug formation, dryout, reverse flow and flow at the exit manifold) during flow boiling of water in a single rectangular mini-channel. Satitchaicharoen and Wongwises [13] studied the flow patterns of vertical upward gas–liquid two-phase flow in mini-gap rectangular channels. The effects of gap size, channel width and liquid viscosity on the flow pattern transitions were examined.

There are some studies dealing with two-phase flow in annuli. Lahey and Ohkawa [14] used the gamma-ray attenuation technique to determine local void fractions of different kinds of gas–liquid flow patterns in vertical annular channels. Kelessidis and Dukler [15] performed vertical upward air–water two-phase flow experiments in a vertical annuli ($D_i = 50.8$ mm, $D_o = 76.2$ mm). Bubbly, slug, churn, annular and annular-with-lumps flow patterns were observed in their experiments. Osamasali and Chang [16] conducted air–water two-phase flow experiments in horizontal annuli with $D_i = 50.8$ mm at various outer diameters ($D_o = 135.4$, 101.6 and 81.9 mm). They could identify five common flow patterns: smooth, wavy, plug, slug and annular. In their experiment, $D_i/D_o$ ratios slightly affected the flow regime transition.

Ekberg et al. [17] conducted an experiment on two-phase flow in narrow channels of horizontal 430 mm-long concentric annular tubes, with inner diameter of outer tube and outer diameter of inner tube of 8.6–6.6 mm and 35.2–33.2 mm, respectively. Air–water was used as the tested fluid, with superficial velocity of air and water within the ranges of 0.02–57 m/s and 0.1–6.1 m/s, respectively. Flow pattern, void fraction and pressure drop within the 250 mm range were investigated. The flow patterns found were slug/plug, stratified-slug, stratified, annular-slug, bubbly-plug, dispersed bubbly, and churn. The stratified flow pattern was not evident in small tube, but it was believed to occur at low air and water flow rates which was not covered in this experiment. A quick valve-closing method was used to find the value of void fraction occurred in the channel from the level of water stored between two valves. The pressure drop was measured within the length of 250 mm using differential pressure transducer.

Up to now, there has been only one work, carried out by Ekberg et al. dealing with two-phase flow in narrow annuli. However, it can be noted that their study concentrated on horizontal flow and no attention was paid to the effects of inclination angles. In the present study, the main objective is to obtain and clarify the characteristics of flow pattern, pressure drop and void fraction in inclined upward co-current gas–liquid two-phase flow in a narrow annular channel. The effect of inclination angle on the flow patterns, flow pattern maps, pressure drop and void fraction, which have never before appeared in open literature, are presented.

## 2. Experimental apparatus and procedure

The schematic diagram of the experimental apparatus is shown in Fig. 1. The main components of the system con-

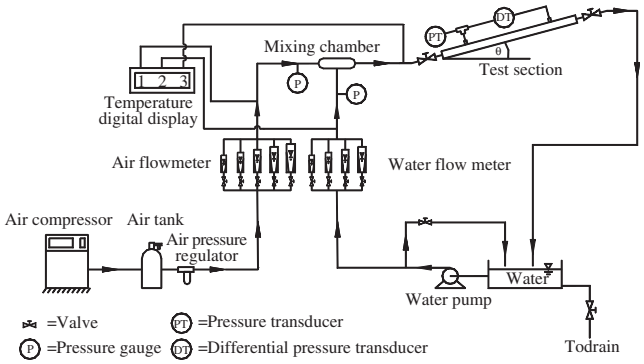


Fig. 1. Schematic diagram of the experimental apparatus.

sisted of a test section (Fig. 2), an air supply, and a water supply. The annular test section with an inner diameter ($D_i$) of 8 mm, outer diameter ($D_o$) of 12.5 mm (Hydraulic diameter ($D_H$) is 4.5 mm) and overall length of 880 mm, made of transparent acrylic glass were used in the present study. Other parts were constructed accurately by machining an ingot of acrylic glass. The ability of wetting/dewetting due to different surface tensions was, therefore, minimized. The inclination angles of the test section are 0°, 30° and 60°. It should be noted that the test section was accurately constructed and is our latest development. It was designed and employed after problems were encountered from several test sections used in previous experiments. The connections of the piping system were designed such that parts could be changed very easily. The water at room temperature and atmospheric pressure from the water tank was pumped through the rotameter, the air–water mixer and the test section. The surplus water was sent back to storage tank through the control valve. Water in the system was controlled by water flow meter with different measure range. The air at room temperature and atmospheric pressure from the air compressor was pumped to the air tank with high pressure. The high-pressured air was sent into the system through the air pressure regulator in order to control the stability of pressure. Air was supplied from a compressor to pass through the reservoir, the regulator, the flow meter, the mixer and the test section.

The air–water mixer was constructed of many small-diameter tubes with 6 mm inside diameter (Fig. 3). Both the air and water were brought together in a mixer and then passed through the test section co-currently. The flow rates of air were measured by five sets of rotameters within

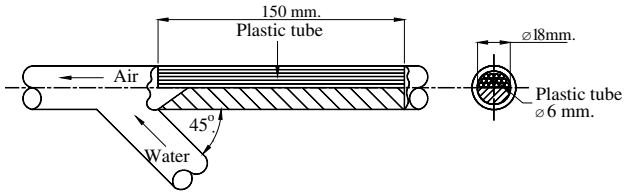


Fig. 3. Schematic diagram of mixing section.

the range of 0.1–1, 1–10, 10–100, 100–500, 600–3000 SCFH, respectively. The flow rates of water were measured by four sets of rotameters within the range of 0.063–0.315, 0.3–1.5, 1–4, 4–36 LPM, respectively. The accuracy of the air and water volumetric flow rates is ±2%. The air–water mixing section served to introduce water smoothly along the test section. The water from the mixer flowed together with air, and then flowed back to the storage tank. Type T thermocouples were used to measure fluid temperatures. The uncertainty of temperature measurements is ±0.1 °C. Air and water pressures at the inlet of the mixer were measured by precision Bourdon tube pressure gauges. The pressure was measured through a tap with a 1.5 mm hole drilled into the tube in which the fluids flow. Two-phase pressure at the inlet of the test section was measured by the pressure transducer calibrated from 0 to 10 bar with a ±20 mbar accuracy. A differential pressure transducer was installed in the test section within the length of 420 mm, to measure the pressure drop across the test section. The range of the transducer was 5–500 kPa. The transducer has an accuracy of ±0.1% of its calibrated span. The averaging time of pressure drop measurements was around 5 s. All pressure taps were mounted flush in the tube wall. Liquid hold-up was measured by using two quickly-closing valves. The uncertainty in the measured liquid hold-up was estimated to be 0.2%. These valves were simultaneously closed to determine the relative volume of air and water trapped. Three samples were taken to obtain the average value. The process of each flow pattern formation was registered in detail by high-speed camera and digital camera.

Experiments were conducted at various air and water flow rates, various inclination angles of the channel. In the experiments, the air flow rate was increased by small increments while the water flow rate was kept constant at a pre-selected value. The system was allowed to approach steady conditions before the air and water flow rates, flow pattern, pressure drop and void fraction were recorded.

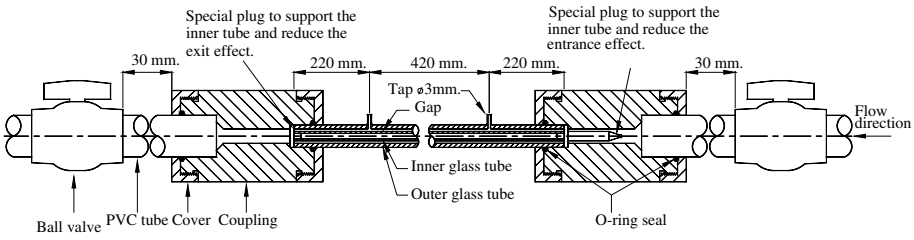


Fig. 2. Schematic diagram of test section.

## 3. Results and discussion

### 3.1. Flow patterns

Visual observations were obtained using a high-speed camera, digital camera and video recorder. Typical photographs and sketches of the observed flow patterns, obtained at the middle of the test section, are shown in Figs. 4–6. These observed flow patterns can be described as follows.

*a. Plug flow (P):* This flow pattern occurs at a relatively low air velocity. The flow pattern is characterized by a continuous stream of elongated bubbles flowing along the upperside of the tube.

*b. Slug flow (S):* At a certain air flow rate, the air–water interface becomes more wavy and unstable. Waves with higher amplitudes grow and block the whole tube section and are then pushed strongly by the air with a very high velocity. Water slugs occasionally pass through the tube with a higher velocity than the bulk of the water. The upstream and downstream portions of water slug are similar to stratified wavy flow.

*c. Annular flow (A):* This flow pattern is characterized by the complete separation of the water and air, with flowing of the water film on the outer and inner tube walls and air in the core.

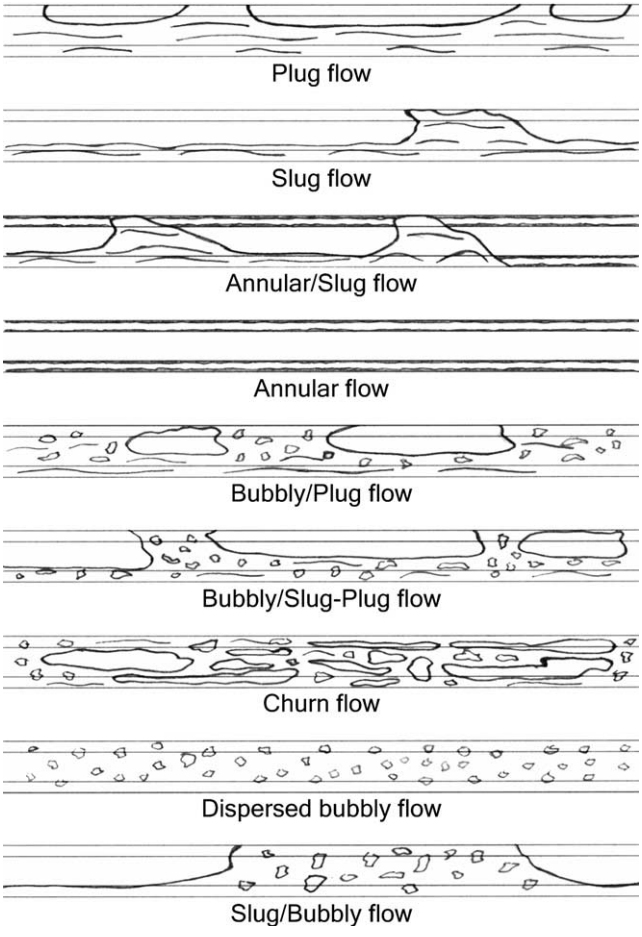


Fig. 4. Sketches of flow patterns.

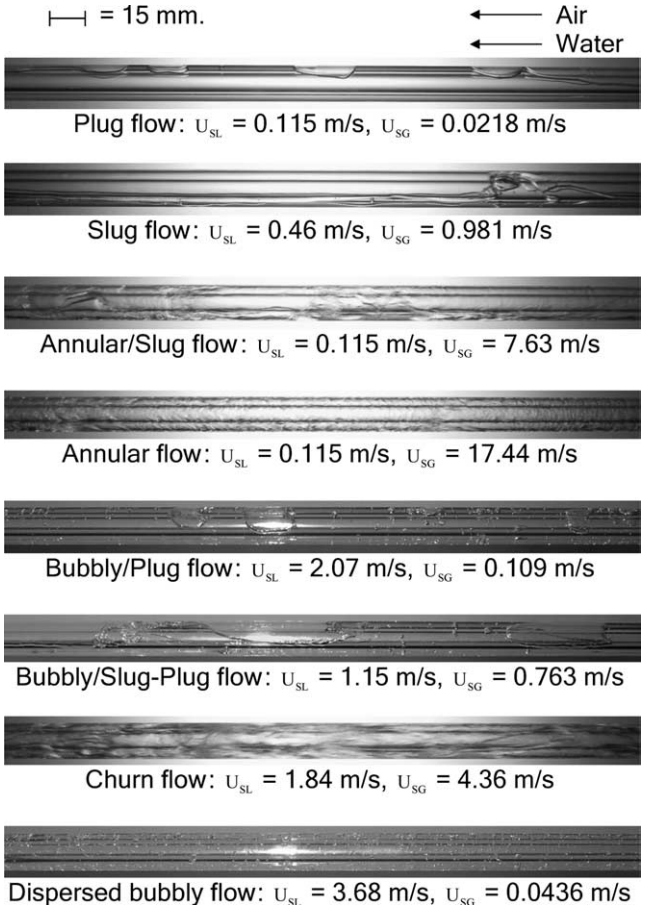


Fig. 5. Flow patterns for $D_o = 12.5$ mm, $D_o = 8.0$ mm, $\theta = 0°$.

*d. Annular/slug flow (A/S):* Formation of the annular/slug flow is similar to that of the annular flow, except for some frequent appearances of water slug.

*e. Bubbly/plug flow (B/P):* With increasing air flow rate, many small bubbles are combined to form "bullet shaped" bubbles. The train of these bubbles follows the channel line in the continuous liquid phase which contains a dispersion of smaller bubbles.

*f. Bubbly/slug–plug flow (B/S–P):* This is similar to the bubbly/plug flow, however due to higher air velocity, larger bubbles are formed through combination of smaller ones. In this flow pattern, slug and plug flow take place by turns and is difficult to be identified.

*g. Churn flow (C):* Churn flow is formed by a breakdown of the slug flow bubbles. This leads to an oscillatory motion, for example, of the liquid downward and upward flows in the inclined tube.

*h. Dispersed bubbly flow (Db):* The flowing liquid phase is continuous and contains a dispersion of small circular-shaped bubbles of various sizes.

*i. Slug/bubbly flow (S/B):* Similar to slug flow, but the liquid slug contains a dispersion of smaller bubbles.

It should be noted that slug flow was found only in the horizontal channel whereas slug/bubbly flow was found

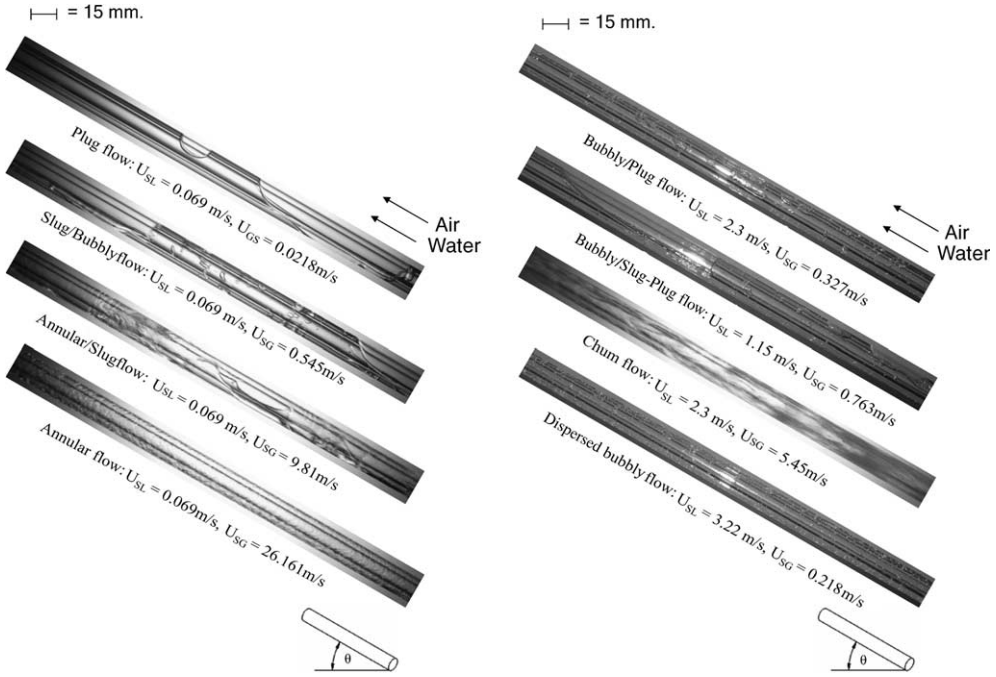


Fig. 6. Flow patterns for $D_o = 12.5$ mm, $D_o = 8.0$ mm, $\theta = 30°$.

only in the inclined channel. The usual method in the presentation of flow pattern data, is to classify the flow pattern by visual observation and plot the data as a flow pattern map in terms of system parameters. Parameters used in the present study are the phase superficial velocities. The superficial velocity of gas ($U_{SG}$) and of liquid ($U_{SL}$) refer to the situation where the designated phase flows alone in the pipe. In the present study, both superficial velocities refer to average ambient conditions (1.013 bar, 30 °C).

Figs. 7–9 show two-phase flow data and flow pattern maps for a test section having $D_i = 8$ mm, $D_o = 12.5$ mm, at $\theta = 0°$, 30° and 60°, respectively. The solid lines in this figure represent the boundary of the flow patterns and transition from one flow pattern to another. Actually, due to the uncertainty at the vicinity of the transitions between flow patterns, the flow patterns do not change suddenly. Therefore, the transition lines should be represented as broad transition bands. The flow pattern map is valid in the range of 0.02–65.50 m/s for $U_{SG}$, and 0.07–6.10 for $U_{SL}$.

In Fig. 10, a comparison is shown of our present flow pattern transitions obtained from the horizontal channel with the measured data of Ekberg et al. [17] obtained from the air–water experiment using horizontal annuli with $D_i = 6.6$ mm and $D_o = 8.6$ mm. The region of plug flow obtained from the present study is in good agreement with the slug/plug flow region obtained from Ekberg et al. All their stratified-slug flow data are in the slug flow region of the present flow pattern map. The annular-slug flow data agrees very well with that of our annular/slug flow region. Most of the annular flow data of Ekberg et al. is located in our annular flow region. The churn flow data of Ekberg et al. also shows significant agreements with respect to our transition lines. Some churn flow data is located in

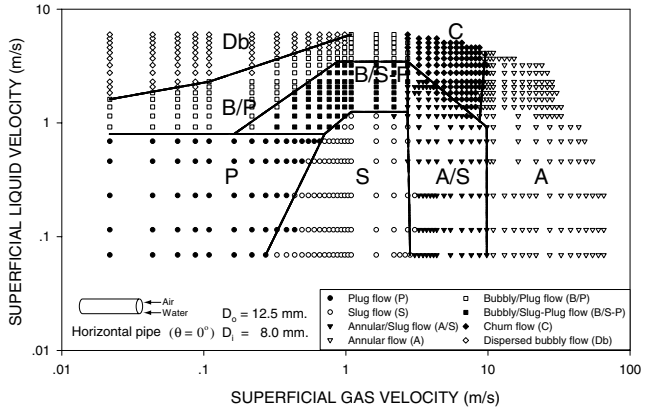


Fig. 7. Present flow pattern map for $D_o = 12.5$ mm, $D_o = 8.0$ mm, $\theta = 0°$.

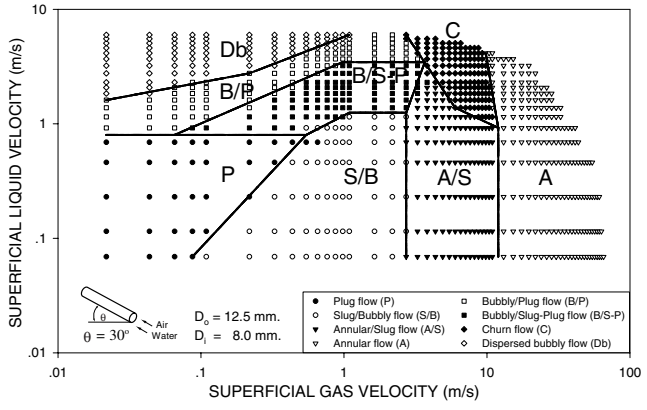


Fig. 8. Present flow pattern map for $D_o = 12.5$ mm, $D_i = 8.0$ mm, $\theta = 30°$.

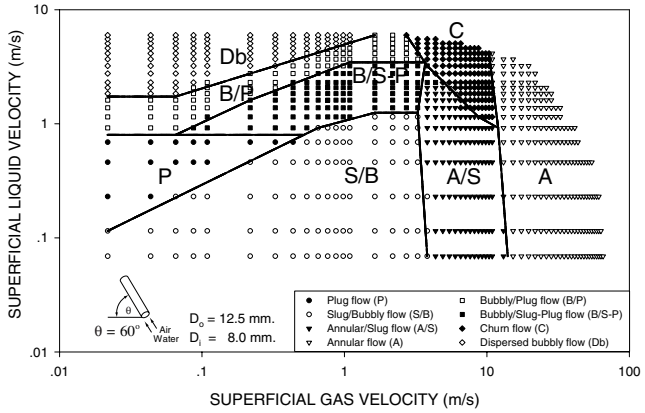


Fig. 9. Present flow pattern map for $D_o = 12.5$ mm, $D_i = 8.0$ mm, $\theta = 60°$.

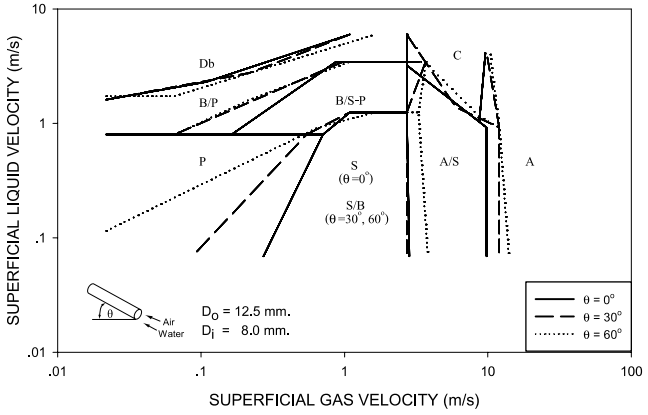


Fig. 11. Effect of inclination angle on the air–water flow pattern map for an annular channel with $D_o = 12.5$ mm, $D_i = 8.0$ mm.

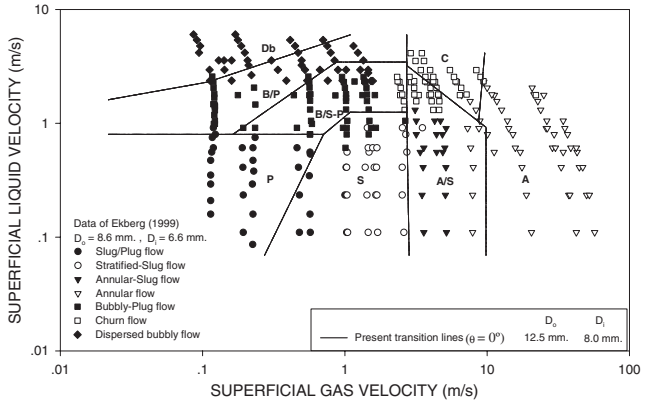


Fig. 10. Present flow pattern map compared with the experimental data of Ekberg et al. [17].

the region of bubbly/slug–plug flow and annular/slug flow in our map. The bubbly–plug flow region of Ekberg et al. is in good agreement with respect to our bubbly/slug–plug flow region. Some dispersed bubbly flow data of Ekberg et al. appear in the bubbly/plug flow region of our flow regime map. Some discrepancies in the comparisons depend mainly on the identification of flow pattern according to their definitions and also the configurations of inlet and outlet sections. However, in general, some parts of the results agree qualitatively.

Fig. 11 shows the flow pattern maps for air–water at different inclination angles. The effect of the inclination angle on the transition lines between the plug flow (P) and the slug flow (S) for $\theta = 0°$, and between the plug flow (P) and the slug/bubbly flow (S/B) for $\theta = 30°$ and 60° are very interesting. At the same superficial water velocity, as a channel with a higher inclination angle was used, the P → S transition line (for $\theta = 0°$) and the P → S/B transition line (for $\theta = 30°$, 60°) shifts to a lower value of superficial air velocity. As the inclination angle increases, the gravitational force increases. As a result, a channel with a higher inclination angle enables the bubbles to be formed at lower air velocity. This is different from the S → A/S (for $\theta = 0°$) and the S/B → A/S (for $\theta = 30°$, 60°), the A/S → A and B/S–P → C transition line, which tend to shift to a higher value of superficial air velocity at the same superficial liquid velocity. In these flow regions, the gravity dominates the flow mechanism. The increase of the air velocity enables the flow pattern to be maintained. It should be noted that, as the inclination angle increases, there are only small shifts of the transition line between the dispersed bubbly flow (Db) and the bubbly/plug flow (B/P), the bubbly/plug flow (B/P) and the bubbly/slug–plug flow (B/S–P), and the bubbly/plug flow (B/P) and the plug flow (P). The plug flow region becomes smaller, while the slug flow region (for $\theta = 0°$) and the slug/bubbly flow region for $\theta = 30°$ and 60° become larger.

### 3.2. Pressure drop

Considering the pressure drop in the horizontal tubes ($\theta = 0°$), it could be seen from Fig. 12 that the pressure drop depends on flow pattern and velocity of gas and liquid. At low liquid velocity, the increase of gas velocity—until the flow pattern changed from plug flow to slug flow—makes the pressure drop increase quickly. This is because when the gas velocity increases, the liquid slug is pushed by the high speed gas to move rapidly, and causes the pressure drop to increase abruptly. When the gas velocity further increases until the flow pattern changes from slug flow to annular/slug flow, the liquid is more replaced by gas and the rise of pressure drop stops. When the gas velocity is high enough to induce sufficient turbulence in the fluid, the pressure drop begins to rise again, due to friction. At higher liquid velocity, on the other hand, the pressure drop rises slowly at first, due to low gas velocity. This is similar to a single-phase flow—i.e., liquid. However, when the gas velocity increases until the flow is sufficiently turbulent, the pressure drop is also risen.

Considering the pressure drop in the tubes with $\theta = 30°$ and 60° as shown in Figs. 13 and 14, it could be seen that at low gas and liquid velocity, the pressure drop during the slug/bubbly flow pattern is not risen abruptly as in the horizontal tubes, because of the effect of gravity. The values of

pressure drop occurred in inclined tubes—at low gas and liquid velocity—are similar at first because the flow at low gas and liquid velocity is not sufficiently turbulent. Hence, the effect of gravity on fluid is more obvious than the friction. However, when the gas velocity increases, the pressure drop also increases. In general, for all inclination angles, the change of pressure drop characteristics corresponded to the flow pattern transitions.

Comparing the pressure drop occurred in the 30°-inclined and 60°-inclined tubes as shown in Fig. 15, it could be seen that—at low gas and liquid velocity—the pressure drop occurred in inclined tubes is higher than the pressure drop occurred in horizontal tubes. This is because at low gas and liquid velocity, the flow is not turbulent enough, due to the obvious effect of gravity on the fluid. When the inclination angle increases, however, the flow becomes more turbulent and makes the effect of friction more prominent. At the same time, the effect of gravity gradually decreases because more liquid is replaced by gas. Consequently, the values of pressure drop occurred in the horizontal, 30°-inclined, and 60°-inclined tubes—at high gas and liquid velocity—are more similar. The pressure

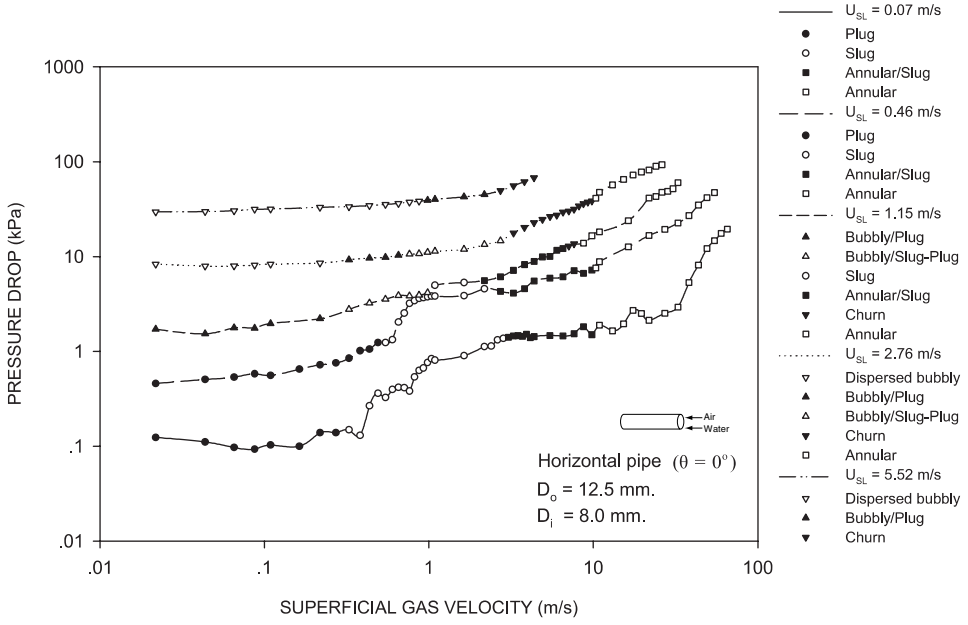


Fig. 12. Relationship between pressure drop and superficial gas velocity for $D_o = 12.5$ mm, $D_i = 8.0$ mm, $\theta = 0°$.

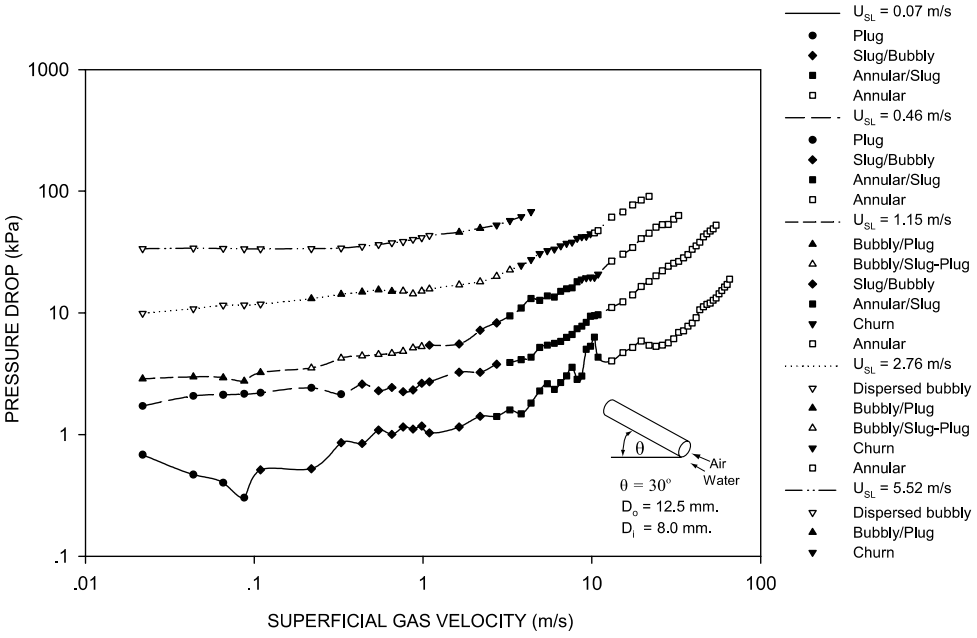


Fig. 13. Relationship between pressure drop and superficial gas velocity for $D_o = 12.5$ mm, $D_i = 8.0$ mm, $\theta = 30°$.

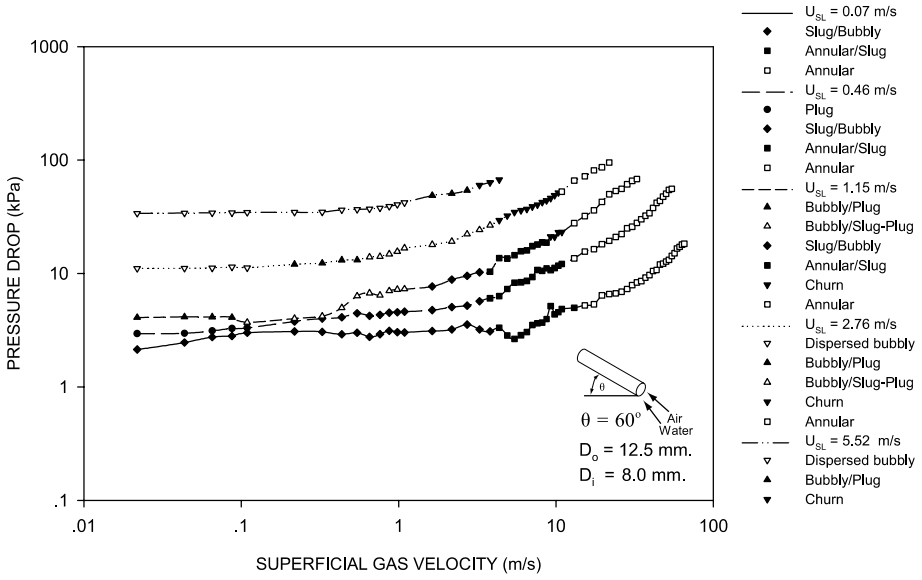


Fig. 14. Relationship between pressure drop and superficial gas velocity for $D_o = 12.5$ mm, $D_i = 8.0$ mm, $\theta = 60°$.

drop in inclined tubes tends to be slightly higher, due to the effect of gravity on fluid inside the inclined tube. The two-phase frictional pressure gradient can be obtained by subtracting the gravitational and accelerational terms from the total experimental pressure gradient. Fig. 16 shows the plot of Martinelli parameter against the two-phase frictional multiplier. In this figure, comparison of experimental data with the Lockhart–Martinelli correlation is shown. The correlation with $C = 5$ and 20 are shown by a solid line. Fig. 17 shows the comparison of the homogeneous flow model (HEM) with experimental data for $\theta = 0°$. There is an overall agreement between the results obtained from the experiment and those obtained from the model.

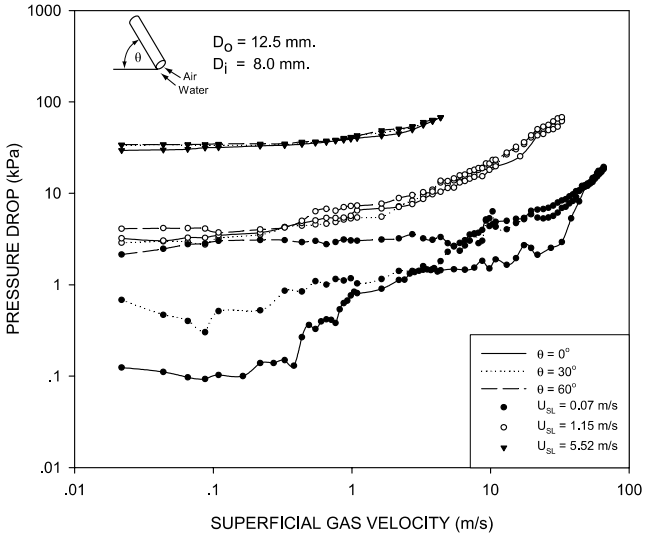


Fig. 15. Relationship between pressure drop and superficial gas velocity for $D_o = 12.5$ mm, $D_i = 8.0$ mm, $\theta = 0°$, 30° and 60°.

### 3.3. Void fraction

From Figs. 18–20, values of void fraction found in the horizontal, 30°-, and 60°-inclined tubes tend to go in the same direction—that is, varied by the values of superficial velocity of both gas and liquid. In other words, void fraction increases when the gas velocity increases. For example, when the fluid changes its flow pattern from annular/slug flow to annular flow (A/S → A), it has to increase its velocity in order to form a liquid film at the tube surface. According to the definition of annular flow, when the gas velocity increases, the liquid part would be increasingly replaced with gas. This causes the increase of void fraction. On the other hand, when the liquid velocity increases, the value of void fraction decrease, due to more replacement of gas with liquid.

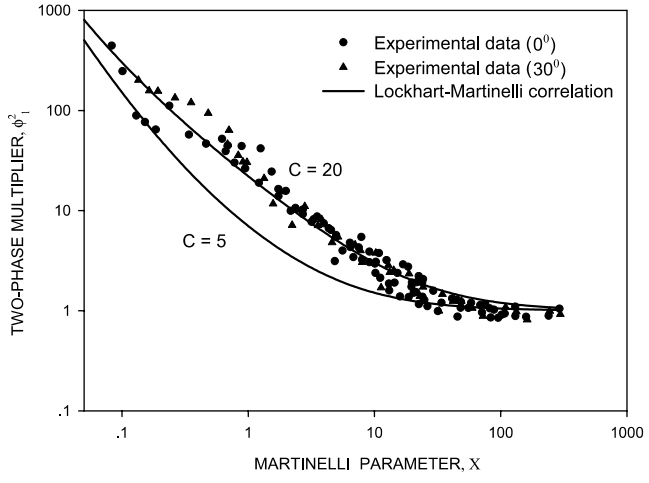


Fig. 16. Martinelli parameter versus the two-phase frictional multiplier.

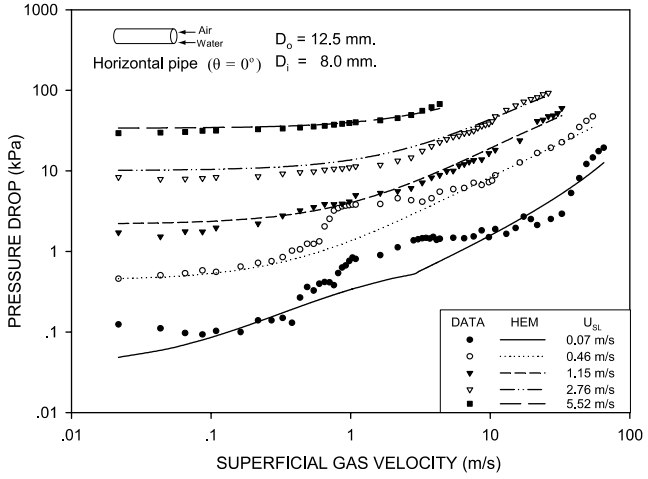


Fig. 17. Comparison of the present data with the prediction.

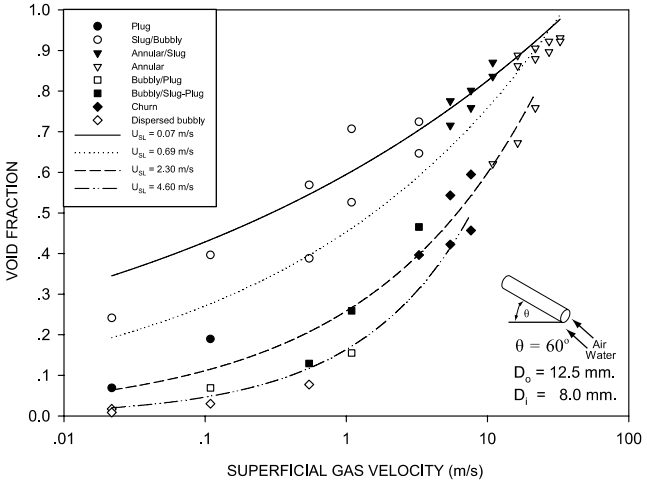


Fig. 20. Relationship between void fraction and superficial gas velocity for $D_o = 12.5$ mm, $D_i = 8.0$ mm, $\theta = 60°$.

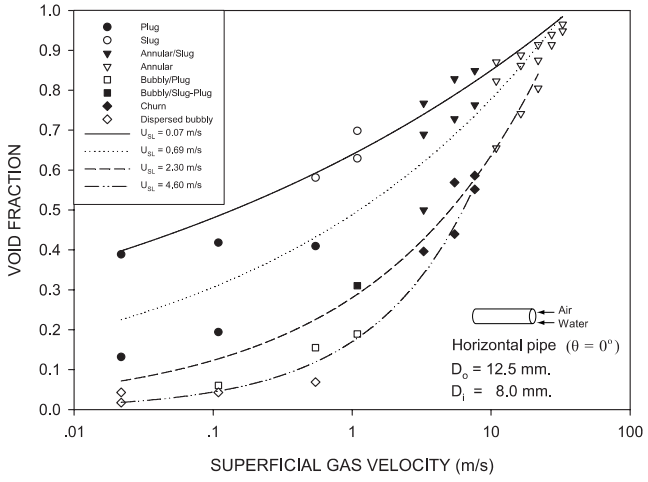


Fig. 18. Relationship between void fraction and superficial gas velocity for $D_o = 12.5$ mm, $D_i = 8.0$ mm, $\theta = 0°$.

From Figs. 18–20, values of void fraction occurred in the tube with $\theta = 0°$, 30° and 60° were similar. However, the value of void fraction seems to decrease when the inclination angle increase, because the liquid was naturally pulled to the bottom by gravity when the inclination angle increases. Some part of liquid may be able to resist the gas flow, which increases amount of water stored in the inclined tubes. Hence, the value of void fraction tends to decrease when the inclination angle increases. Fig. 21 shows the plot of Martinelli parameter against the measured void fraction. It can be clearly seen that void fraction approaches 1 when Martinelli parameter is decreased. Fig. 22 shows the comparison of the correlation proposed by the CISE group (Premoli et al. [18]) with the present measured data. The results obtained from the model show reasonable agreement with the experimental data at high superficial velocity of water. It should be noted that several mathematical models were evaluated in our study. However, only the best one is presented.

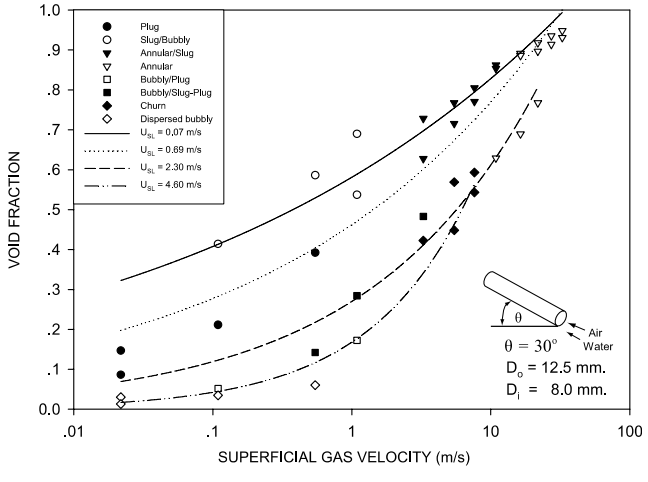


Fig. 19. Relationship between void fraction and superficial gas velocity for $D_o = 12.5$ mm, $D_i = 8.0$ mm, $\theta = 30°$.

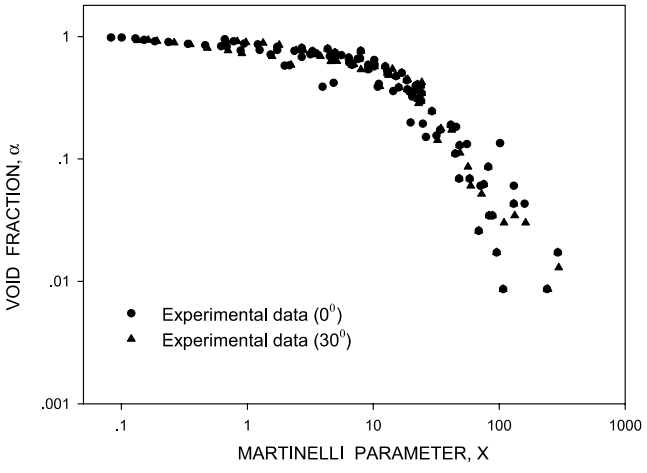


Fig. 21. Martinelli parameter versus void fraction.

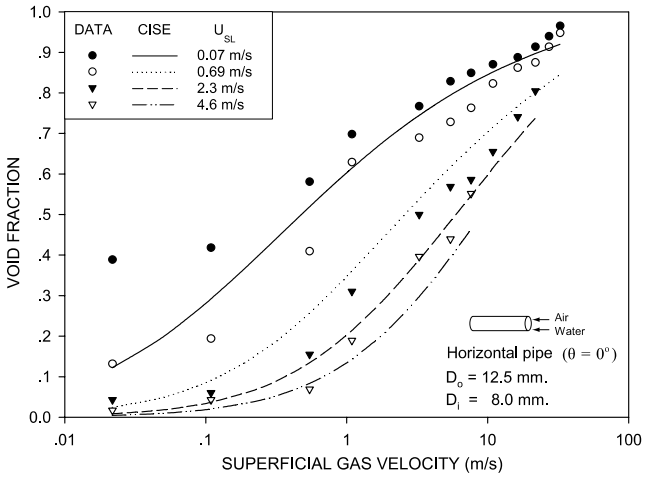


Fig. 22. Comparison of the present data with the prediction.

## 4. Conclusion

The experimental results of flow pattern, void fraction and pressure drop of gas–liquid flow in a narrow concentric annular channel were presented. The annular transparent test section with an inner diameter of 8 mm, outer diameter of 12.5 mm, and overall length of 880 mm was used. The inclination angles of the test section ($\theta$) were 0°, 30° and 60°. Air and water were used as working fluids. The gas superficial velocity and liquid superficial velocity were varied in a range of 0.0218–65.4 m/s and 0.069–6.02 m/s, respectively. The plug, slug, annular/slug, annular, bubbly/plug, bubbly/slug–plug, churn, slug/bubbly and dispersed bubbly two-phase flow patterns were observed in the experiments. The slug/bubbly flow pattern was found only in the case of $\theta = 30°$ and 60°, while the slug flow pattern was found only in the horizontal channel. The experimental results showed that the inclination angle has a significant effect on the flow pattern transition, pressure drop and void fraction. Several existing models were used to compare calculations with the experimental data. However, in the present paper, the best ones were proposed. For $\theta = 0°$, the homogeneous flow model (HEM) gave the overall agreement with the measured pressure drop data while the CISE correlation gave reasonable agreement with the void fraction data.

## Acknowledgement

The present study was financially supported by the Thailand Research Fund (TRF) whose guidance and assistance are gratefully acknowledged.

## References

[1] L. Zhao, K.S. Rezkallah, Gas–liquid flow patterns at microgravity condition, International Journal Multiphase Flow 19 (1993) 751–763.
[2] T. Wilmarth, M. Ishii, Two-phase flow regime in narrow rectangular vertical and horizontal channels, International Journal of Heat and Mass Transfer 37 (1994) 1749–1758.
[3] T. Wilmarth, M. Ishii, Interfacial area concentration and void fraction of two-phase flow in narrow rectangular vertical channels, Journal of Fluid Engineering 19 (1997) 916–922.
[4] J. Bonjour, M. Lallemand, Flow patterns during boiling in a narrow space between two vertical surfaces, International Journal of Multiphase Flow 24 (1998) 947–960.
[5] J. Xu, Experimental study on gas–liquid two-phase flow regimes in rectangular channels with mini gaps, International Journal of Heat and Fluid Flow 20 (1999) 422–428.
[6] J. Xu, P. Cheng, T.S. Zhao, Gas–liquid two-phase flow regimes in rectangular channels with mini/micro gaps, International Journal of Multiphase Flow 25 (1999) 411–432.
[7] T. Hibiki, K. Mishima, Flow regime transition criteria for upward two-phase flow in vertical narrow rectangular channels, Nuclear Engineering and Design 203 (2001) 117–131.
[8] K. Mishima, M. Ishii, Flow regime transition criteria for upward two-phase flow in vertical tubes, International Journal of Heat and Mass Transfer 27 (1984) 723–737.
[9] T.S. Zhao, Q.C. Bi, Co-current air–water two-phase flow patterns in vertical triangular micro-channels, International Journal of Multiphase Flow 27 (2001) 765–782.
[10] M.K. Akbar, D.A. Plummer, S.M. Ghiaasiaan, On gas–liquid two-phase flow regimes in micro-channels, International Journal of Multiphase Flow 29 (2003) 855–865.
[11] K.S. Rezkallah, Weber number based flow pattern maps for liquid–gas flows at microgravity, International Journal of Multiphase Flow 22 (1996) 1265–1270.
[12] P. Balasubramanian, S.G. Kandlikar, High speed photographic observation of flow patterns during flow boiling in single rectangular minichannel, ASME Summer Heat Transfer Conference July 21–23, 2003, Las Vegas, Nevada, USA.
[13] P. Satitchaicharoen, S. Wongwises, Two-phase flow pattern maps for vertical upward gas–liquid flow in mini-gap channels, International Journal of Multiphase Flow 30 (2004) 225–236.
[14] R.T. Lahey, K. Ohkawa, An experimental investigation of phase distribution in an eccentric annulus, International Journal of Multiphase flow 15 (1989) 447–457.
[15] V.C. Kelessidis, A.E. Dukler, Modeling flow pattern transitions for upward gas–liquid flow in vertical concentric annuli, International Journal of Multiphase Flow 15 (1989) 173–191.
[16] S.I. Osamasali, J.S. Chang, Two-phase flow regime transition in a horizontal pipe and annulus flow under gas–liquid two-phase flow, ASME FED 72 (1988) 63–69.
[17] N.P. Ekberg, S.M. Ghiaasiaan, S.I. Abdel-Khalik, M. Yoda, S.M. Jeter, Gas–liquid two-phase flow in narrow horizontal annuli, Nuclear Engineering and Design 192 (1999) 59–80.
[18] A. Premoli, D. Francesco, A. Prina, A dimensionless correlation for determining the density of two-phase mixtures, Lo Termotecnica 25 (1971) 17–26.